1-1-2019

Residual trapping of CO2 in an oil-filled, oil-wet sandstone core: Results of three-phase pore-scale imaging

Stefan Iglauer
Edith Cowan University, s.iglauer@ecu.edu.au

Adriana Paluszny

Taufiq Rahman

Yihuai Zhang

Wolfgang Wülling
Edith Cowan University, w.wuelling@ecu.edu.au

See next page for additional authors

10.1029/2019GL083401
Iglauer, S., Paluszny, A., Rahman, T., Zhang, Y., Wülling, W., & Lebdev, M. (2019). Residual trapping of CO2 in an oil-filled, oil-wet sandstone core: results of three-phase pore scale imaging. *Geophysical Research Letters, 46*(20), 11146-11154. Available here

Geophysical Research Letters

RESEARCH LETTER
10.1029/2019GL083401

Residual Trapping of CO_2 in an Oil-Filled, Oil-Wet Sandstone Core: Results of Three-Phase Pore-Scale Imaging

Stefan Iglauer[1], Adriana Paluszny[2], Taufiq Rahman[3], Yihuai Zhang[4], Wolfgang Wülling[1], and Maxim Lebedev[5]

[1]School of Engineering, Edith Cowan University, Joondalup, Western Australia, Australia, [2]Department of Earth Science and Engineering, Imperial College London, London, UK, [3]Department of Petroleum Engineering, Curtin University, Kensington, Western Australia, Australia, [4]Lyell Centre, Heriot-Watt University, Edinburgh, UK, [5]Department of Exploration Geophysics, Curtin University, Kensington, Western Australia, Australia

Key Points:
- CO_2 was injected into an oil-wet, oil-filled sandstone core and imaged via μCT to determine residual trapping
- Substantial amounts of CO_2 were residually trapped
- Oil extraction was enhanced during a post-CO_2-injection water flood

Supporting Information:
- Supporting Information S1

Correspondence to:
S. Iglauer,
s.iglauer@ecu.edu.au

Citation:
Iglauer, S., Paluszny, A., Rahman, T., Zhang, Y., Wülling, W., & Lebedev, M. (2019). Residual trapping of CO_2 in an oil-filled, oil-wet sandstone core: Results of three-phase pore-scale imaging. *Geophysical Research Letters*, *46*, 11,146–11,154. https://doi.org/10.1029/2019GL083401

Received 23 APR 2019
Accepted 4 AUG 2019
Accepted article online 19 AUG 2019
Published online 21 OCT 2019

Abstract CO_2 geosequestration in oil reservoirs is an economically attractive solution as it can be combined with enhanced oil recovery (CO_2-EOR). However, the effectiveness of the associated three-phase displacement processes has not been tested at the micrometer pore scale, which determines the overall reservoir-scale fluid dynamics and thus CO_2-EOR project success. We thus imaged such displacement processes in situ in 3-D with X-ray microcomputed tomography at high resolution at reservoir conditions and found that oil extraction was enhanced substantially, while a significant residual CO_2 saturation (13.5%) could be achieved in oil-wet rock. Statistics of the residual CO_2 and oil clusters are also provided; they are similar to what is found in analogue two-phase systems although some details are different, and displacement processes are significantly more complex.

1. Introduction

CO_2 geostorage combined with enhanced oil recovery (CO_2-EOR) is an attractive and economic solution for reducing anthropogenic greenhouse gas emissions and mitigating global warming (Cantucci et al., 2009; Emberley et al., 2005; Intergovernmental Panel on Climate Change, 2005). The targeted oil reservoirs, however, are typically oil wet (Cuiec, 1991), which drastically reduces residual (Al-Khdheeawi et al., 2017; Al-Menhali et al., 2016; Al-Menhali & Krevor, 2016; Chaudhary et al., 2013; Iglauer, 2017; Krevor et al., 2015; Rahman et al., 2016) and structural (Naylor et al., 2011; Iglauer, Al-Yaseri, et al., 2015; Iglauer, Pentland, & Busch, 2015; Iglauer, 2017; Arif et al., 2017) trapping capacities and significantly accelerates vertical CO_2 migration (Al-Khdheeawi et al., 2017), which is detrimental as the injected CO_2 must not leak back to the surface.

It is, therefore, of key importance to quantify how much CO_2 can be safely stored in such oil reservoirs and how CO_2 migrates through the formation. However, such a three-phase (oil, water—which is always present in subsurface formations—and CO_2, which is injected for disposal) system has not been tested at the pore scale (micrometer scale), despite the fact that pore-scale flow determines hectrometre-scale reservoir behavior (Bear, 1988; Sahimi, 2011; Blunt, 2017) and thus the success of any CO_2-EOR project.

Consequently, there is a serious lack of data and understanding of the fundamental in situ parameters and phenomena governing this process, which generates high uncertainty in terms of storage capacity and containment security predictions, translating into increased project risk.

We thus imaged such three-phase (oil/water/CO_2) displacement sequences via high-resolution in situ 3-D X-ray microcomputed tomography (μCT) at reservoir conditions and measured how much CO_2 is trapped as a residual phase in oil-wet rock and how much additional oil is produced. A statistical analysis of the residual phases is also provided. Results show that CO_2 effectively enhances oil production, remaining partially trapped in the core plug thereafter.

2. Experimental Procedure

2.1. Mimicking an Oil Reservoir at Laboratory Scale

It is well established that mimicking true reservoir conditions (i.e., high pressure and elevated temperature) in laboratory-scale experiments is required to achieve representative measurements (Iglauer & Lebedev,

Table 1
Interfacial Tensions of the Fluids Used

Fluid-fluid system	Interfacial tension (mN/m)
Water-CO_2[a]	39.5
Water-1-Bromododecane[b]	22.8
1-Bromododecane-CO_2[c]	2.8

[a]Measured at 323 K and 10 MPa for 0.98 M (0.864 NaCl + 0.136 KCl) brine (Li et al., 2012). [b]Measured at 330.89 K and 8.851 MPa for Ontario crude oil-Saskatchewan reservoir brine (4,270-mg/L total dissolved solids; Yang et al., 2005). [c]Measured at 330.74 K and 13.362 MPa for Ontario crude oil (Yang et al., 2005).

2018). This is due to the CO_2 being in a supercritical state, in which it has an increased viscosity, a strongly increased density, and, importantly, also a strongly enhanced CO_2-rock wettability (e.g., Al-Yaseri et al., 2016a, 2016b; Span & Wagner, 1996; Yang et al., 2008a, 2008b).

Thus a sandstone oil reservoir at a depth of approximately 1,000 m (10-MPa pore pressure and 323-K temperature) was simulated in the laboratory. A clean homogeneous sandstone (Bentheimer) was selected, and small core plugs (5-mm diameter and 10-mm length) were drilled. The whole flood sequence was imaged for one miniature plug only. Porosity was 21.5% ± 0.5%, permeability 2,047 ± 27 mD (Saenger et al., 2016), and the rock consisted of 99 wt% quartz, 0.7 wt% kaolinite, and 0.3 wt% rutile. Initially, this rock was completely water wet at ambient conditions (0° water contact angle in air); however, oil reservoir rock is frequently oil wet (Cuiec, 1991). We thus rendered the plug oil wet (130° water contact angle measured at ambient conditions in air, cf. Rahman et al., 2016) by immersing it into silane (Dodecyltriethoxysilane, ≥99.9 mol% purity, from Sigma-Aldrich) under vacuum and subsequently aged the plug for four weeks at ambient conditions (cp. Al-Anssari et al., 2016, Nwidee et al., 2016; Rahman et al., 2016). This process guarantees strongly oil-wet conditions in a highly reproducible way.

2.2. Pore-Scale μCT Imaging

The oil-wet plug was then placed into an X-ray transparent high-pressure μCT cell (Iglauer & Lebedev, 2018) and vacuumed for 4 hr to remove all air from the system. Subsequently oil (1-Bromododecane, which has a high CT contrast, purity ≥ 98 mol%, from Sigma-Aldrich) was injected so that the plug was fully oil saturated, and the pore pressure was raised to 10 MPa, the confining pressure to 15 MPa, and all flow lines and fluids were isothermally heated to 323 K. This was followed by injection of 50 pore volumes (PV) of water (using doped "dead" brine; i.e., 7 wt% NaI in deionized water; note that NaI is required for CT contrast) at a capillary number ($N_{cap} = v\mu/\gamma$, where v is the Darcy velocity of the injected fluid, μ is the viscosity of the injected fluid, and γ is the fluid-fluid interfacial tension) of 3.72×10^{-7}, which was followed again by a second oil flood (50 PV of oil were injected again at a capillary number of 9.87 x 10^{-6}) so that a water-oil two-phase system was created, which represents an (oil-wet) oil reservoir at connate water saturation (S_{wc}) at approximately 1,000 m depth. The core plug was then imaged at S_{wc} in 3D at a resolution of $(3.4\ \mu m)^3$ with an Xradia VersaXRM μCT instrument. Afterwards 40 PV of supercritical (sc) CO_2 were injected at a flow rate of 0.1 mL/min, which corresponded to a capillary number of 6×10^{-8}, and the core was imaged again at initial CO_2 saturation (S_{gi}). Finally 40 PV of CO_2-saturated "live" brine (i.e., brine thermodynamically equilibrated with CO_2 at 10 MPa and 323 K; El-Magrhaby et al., 2012) were injected at a flow rate of 0.1 mL/min ($N_{cap} = 3.72 \times 10^{-7}$), and the sample was μCT imaged again at residual CO_2 saturation (S_{gr}). The interfacial tensions (γ) of the fluids used are tabulated in Table 1, and the related spreading coefficient of the oil was $S_{spreading} = \gamma_{gw} - \gamma_{ow} - \gamma_{og} = 13.9$ mN/m; thus, the oil tended to spread out on the water.

The μCT images were filtered with a 3-D nonlocal means algorithm (Buades & Morel, 2005) and segmented with a watershed algorithm (Schlüter et al., 2014). Petrophysical properties were then measured on the 3-D images; see below.

3. Results and Discussion

3.1. Fluid Saturations and Pore-Scale Configurations

For CO_2 geostorage project assessment it is crucial to know how much CO_2 can be stored as a residual phase (Krevor et al., 2015). Indeed, some geostorage projects have been approved solely on the basis of this storage mechanism (Stalker et al., 2013). Similarly, it is vital to know how much additional oil can be produced by CO_2 injection (Lake, 2010). This information forms the basis of economic decisions in terms of whether CO_2-EOR schemes are feasible (Green & Willhite, 1998; Lake, 2010). Technically, this information is quantified by the fluid saturation S (i.e., the volume fraction a fluid occupies in the pore space of the rock) and S can be measured on the μCT images for the three fluids (oil: S_o; water: S_w; CO_2: S_{CO2}), Iglauer and Lebedev (2018).

Initially, the plug contained 64.5% oil (Table 2 and Figures 1 and S1 in the supporting information) in the pore space at connate water saturation (S_{wc}). This was mainly due to the strongly oil-wet rock surface, which led to oil (the wetting phase) residing in the smallest pores and thus a high oil saturation (S_o). Water was present only in the large pores as it was the nonwetting phase (Øren & Pinczewski, 1995; Piri & Blunt, 2004; Soll et al., 1993); however, due to its residence in the larger pores, water saturation was significant (S_w = 35.5%). The roundish shape of the water drops was caused by interfacial forces, which minimized the droplet's surface areas (sometimes distorted by pore geometry) and with that the (Gibbs) energy of the system.

This configuration represents an oil-wet oil reservoir where the capillary pressure of water is relatively low, that is, more at the top or in the center of the oil column (Watts, 1987). During CO_2 injection (CO_2 is the intermediate-wetting phase; cf Figure 1), most of these water drops were displaced by $scCO_2$. The $scCO_2$ moved into large but also intermediate-sized pores, so that an initial $scCO_2$ saturation of 41.3% was achieved, and a significant amount of oil (oil recovery factor $R_{CO2\text{-}flood} = \frac{S_o \text{ produced by CO2 flooding}}{S_o \text{initial}} = \frac{19.1\%}{64.5\%} = 29.6\%$) was recovered. The CO_2 bubbles were again roundish due to interfacial forces. From Figure 1 it can be inferred that two pore-scale displacement processes occurred, namely, (a) a two-phase direct drainage process, where CO_2 directly displaced oil, and (b) a three-phase double-drainage process (Øren & Pinczewski, 1994, 1995), where CO_2 displaced water, which again displaced oil. This is similar to displacement processes found in N_2 injection processes once the ranking of the fluid phases with respect to their mineral surface wetting affinity is taken into account (i.e., N_2 is the nonwetting phase there and water is the wetting phase if the rock is water-wet; Scanziani et al., 2018; Khishvand et al., 2016; Iglauer et al., 2013, 2016).

Subsequently, when water was injected to residually trap CO_2 and to produce more oil, approximately 70% of the CO_2 was displaced by the water, and water remained mainly in spaces, which were previously occupied by CO_2 (Figure 1). This, in combination with the CO_2 phase morphology (cf. Figure S1), indicates that CO_2—as the intermediate-wet phase—is sandwiched between the oil and water phases. Thus, CO_2 has a layer-like structure, which has also been observed previously for the intermediate-wetting phase in analogue systems (e.g., Iglauer et al., 2013; Scanziani et al., 2018); it is therefore possible that more of this CO_2 is displaced as such layers can attain very thin thicknesses, although the relative permeability of such a thin layer would be very low (Keller & Chen, 2003). In addition, it is apparent from Figure 1 that now three displacement processes occurred, namely, (a) water displaced CO_2 directly in a two-phase drainage process, (b) water also displaced additional oil directly in a two-phase drainage process, and (c) water displaced CO_2, which again displaced more oil in a double-drainage process. This is somewhat different to what has been observed previously for N_2 systems, as there waterflooding corresponds to an imbibition process (Scanziani et al., 2018). Note that oil is hydraulically connected throughout all flooding sequences. Overall, however, significant amounts of residual CO_2 (13.5%) were stored, and a substantial amount of additional oil (18.6%) was recovered by waterflooding ($R_{waterflood} = = \frac{S_o \text{ produced by waterflooding}}{S_o \text{ initial}} = \frac{12.0\%}{64.5\%} = 18.6\%$; Table 2).

Thus, in summary, when compared with analogous two-phase (water/CO_2) experiments (Al-Menhali et al., 2016; Andrew et al., 2013, 2014; Chaudhary et al., 2013; Iglauer et al., 2011; Rahman et al., 2016), it is clear that overall less CO_2 can be stored in oil-wet rock by residual trapping; however, it was demonstrated on the miniature core plug used here that a similar amount of CO_2 can be stored in three-phase systems (i.e., oil reservoirs, as opposed to aquifers). The 3-D fluid morphologies reflect this (Figure S1 in the supporting information); these phase structures were further statistically analyzed in detail in section 3.2 below.

3.2. Residual Cluster Statistics

3.2.1. Oil and CO_2 Cluster Size Distributions

Subsequently, the oil and CO_2 cluster size distributions were analyzed as they are related to remobilization and mass transfer effects. Larger clusters can be remobilized more easily (Herring et al., 2013), and they have a smaller surface area-to-volume ratio, which slows down mass transfer (Iglauer & Wülling, 2016; Jiang et al., 2016). Note that remobilization of CO_2 needs to be avoided (as it increases leakage risk), and mass transfer needs to be accelerated to maximize dissolution trapping—a safe storage mechanism where CO_2 dissolves in formation brine and sinks deep into the reservoir (Al-Khdheeawi et al., 2017; Emami-Meybodi et al., 2015).

Table 2
Water, Oil, and CO_2 Saturations in the Oil-Wet Bentheimer Sandstone at 323 K and 10-MPa Pore Pressure at Various Saturation States

Saturation state	Water saturation (%)	Oil saturation (%)	CO_2 saturation (%)
Connate water (S_{wc})	35.5	64.5	0
Initial CO_2 (S_{gi})	13.2	45.4	41.4
Residual CO_2 (S_{gr})	53.1	33.4	13.5

We thus analyzed these cluster distributions by counting the number N of oil or CO_2 clusters of size (volume) V. The normalized frequency (=N/total number of oil/CO_2 clusters) is plotted against cluster size for each saturation state, Figure 2.

Clearly, N always dropped rapidly with increasing cluster size V, consistent with observations made in similar experiments (e.g., Iglauer et al., 2010, 2011, 2013, 2016; Iglauer & Wülling, 2016; Georgiadis et al., 2013; Andrew et al., 2014; Geistlinger et al., 2014; Geistlinger & Mohammadian, 2015). These cluster size distributions followed power law correlations ($N \sim V^{-\tau}$; Table 3). More smaller oil clusters were counted after each flooding step, and, related to that, the cluster size distribution exponent τ significantly increased (from 1.09 to 1.35 after waterflooding, Table 3). This indicates that during the floods, larger oil clusters were split into smaller clusters, consistent with the images shown in Figures 1 and S1. A similar effect was observed for the CO_2 clusters. The initially largest CO_2 cluster was reduced from 1.45×10^9 μm^3 to 3.47×10^7 μm^3 after waterflooding, while the cluster size exponent τ increased from 1.10 to 1.20 (Table 3). Note that an increased τ value implies a higher frequency of smaller CO_2 bubbles, which dissolve quicker in the oil or water phase due to the increased surface-to-volume ratio (Iglauer & Wülling, 2016), thus accelerating dissolution and mineral CO_2 trapping.

3.2.2. Oil and CO_2 Cluster Surface Areas

The cluster surface area-volume relationship is another morphological descriptor of the individual fluid phases, and they provide information directly relevant for any mass transfer considerations (see above). Thus, the interfacial areas A for each CO_2 and oil cluster were measured and plotted against their volume V; from the (log-log) graphs power law relations are evident ($A \sim V^p$; Figure 2) and as with all other measurements of this kind (Iglauer et al., 2013; Karpyn et al., 2010; Pentland et al., 2012), p was always ~0.8. Note that $p = 2/3$ for a sphere, the most compact object, while it is $p \sim 1$ for a percolation-like cluster (Stauffer, 1979). The fluid clusters are therefore less compact than spheres as they can occupy more than one pore (cf. Figures 1 and S1) but less ramified than percolation clusters. Furthermore, p was independent of the fluid and process step.

It is interesting to note that the power law exponents measured (τ and p) are significantly lower than predicted by percolation theory [which predicts $\tau = 2.189$ and $p \approx 1$; Stauffer, 1979; Lorenz & Ziff, 1998]. We thus conclude that simple percolation models are unlikely to deliver reliable predictions; see also Iglauer and Wülling (2016).

3.3. CO_2 and Oil Cluster Capillary Pressure Distributions

Finally, the capillary pressures (p_c)—which strongly influence the multiphase flow behavior through the rock (Blunt, 2017; Øren et al., 1992; Sahimi, 2011; Soll et al., 1993)—of all oil and CO_2 clusters were determined. Thus, the curvature (C) of each cluster was measured on the μCT images, and the associated capillary pressures ($p_c = \gamma C$) were calculated using the CO_2-oil and water-oil interfacial tensions (Table 1), as both, CO_2 and water, were (mainly) surrounded by oil. The accuracy of these measurements is discussed in the supporting information; note that due to the voxelized image acquired in a μCT experiment, a measurement bias is introduced that results in a high count of zero curvatures (and thus zero capillary pressures). This is thus an artifact of the μCT technology and should not be interpreted as a mixed-wet condition (the core is strongly oil wet, see section 2.1).

The capillary pressure distributions were roughly axially symmetric and bell tower shaped and always showed a narrow and high peak at zero capillary pressure (Figure 3), consistent with data reported for oil-water (Armstrong et al., 2012) and three-phase oil-water-gas (Iglauer et al., 2016) systems. Interestingly, the p_c range for the oil clusters at S_{wc} approximately doubled after CO_2 flooding, from approximately

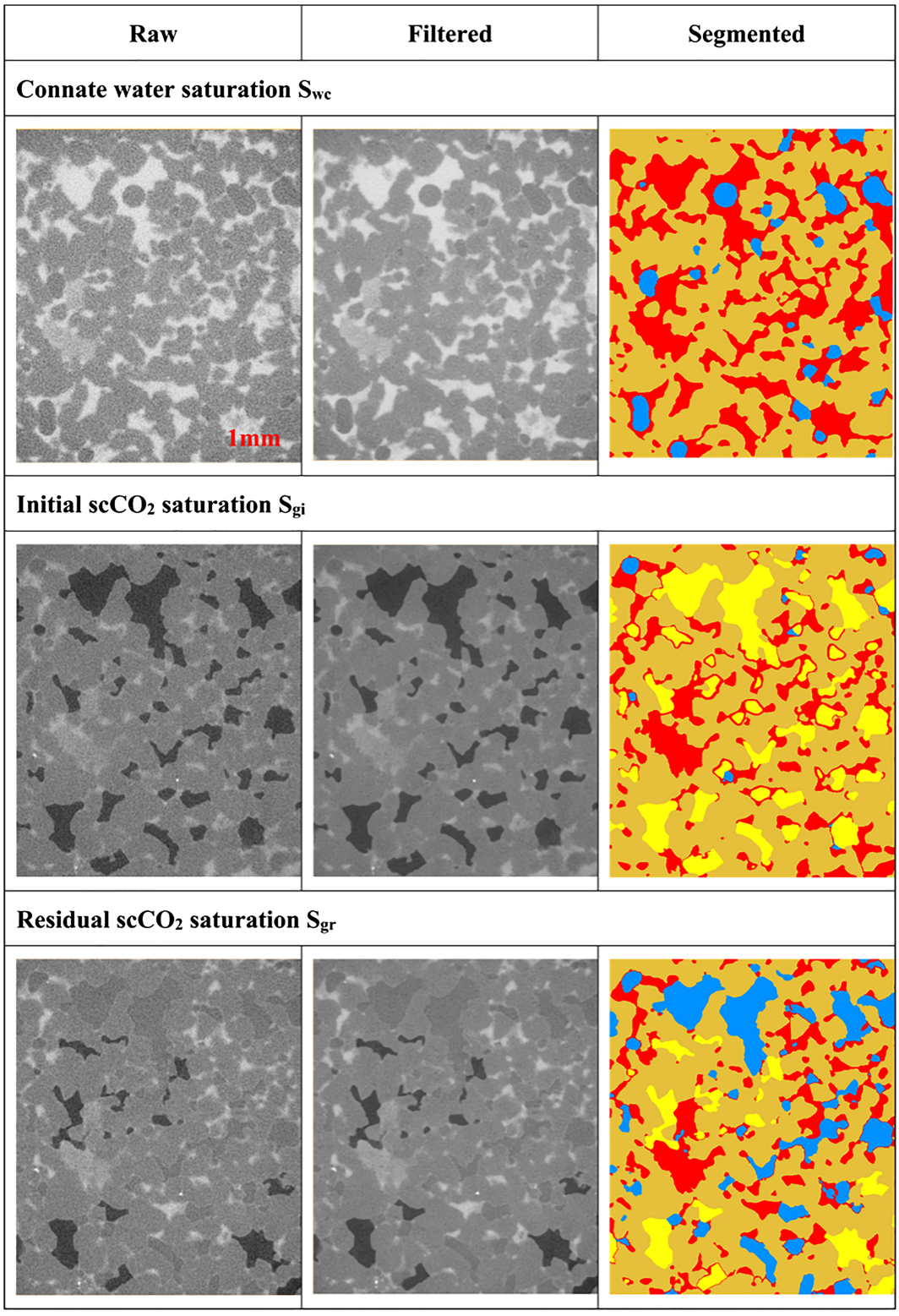

Figure 1. Two-dimensional slices through the rock and various fluids at different saturation states. In the raw and filtered images, oil is white, CO_2 is black, brine dark gray, and sandstone is light gray. Oil is red, brine blue, gas yellow, and rock is brown in the segmented images.

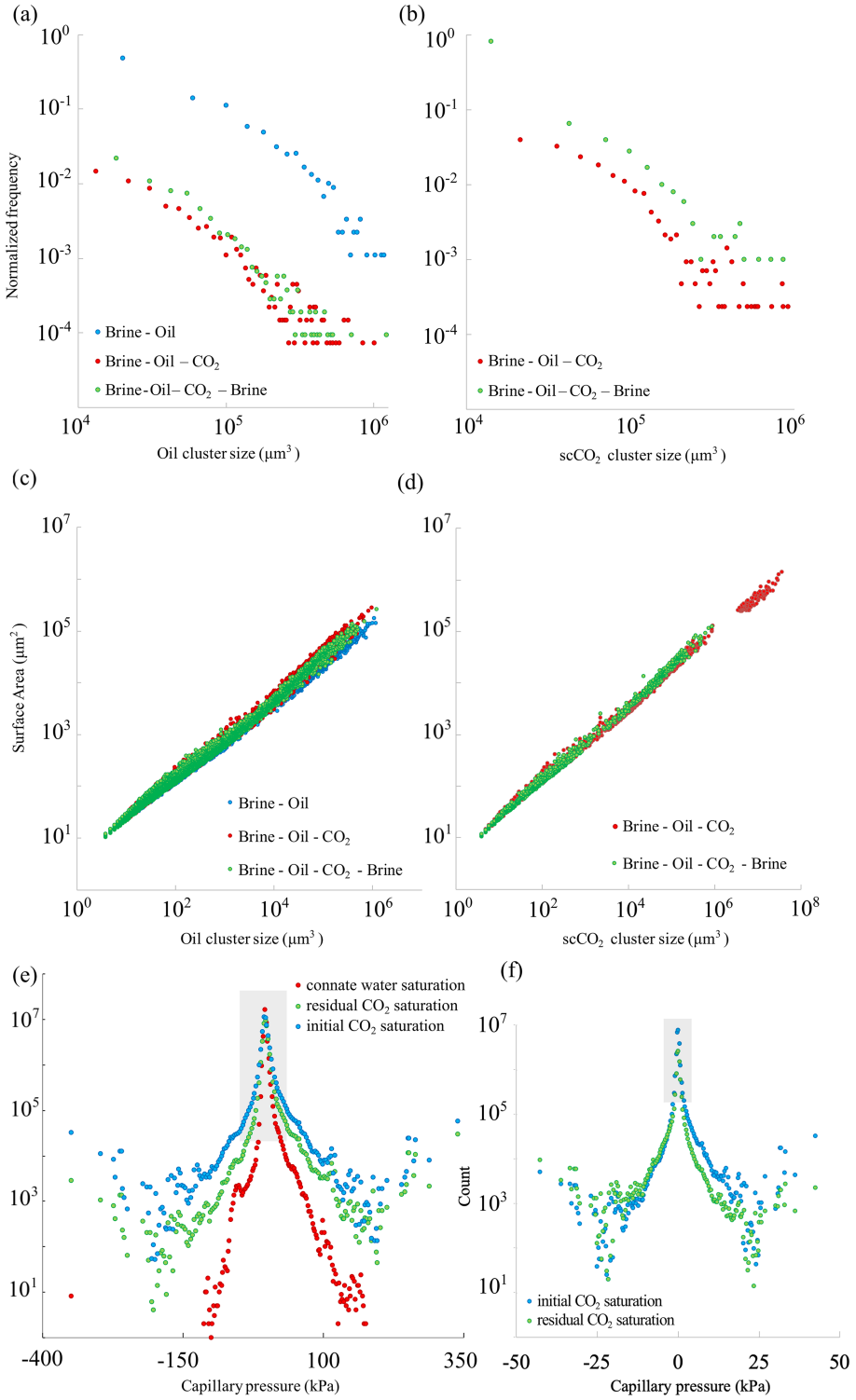

Figure 2. Oil (a) and $scCO_2$ (b) cluster size distribution for each saturation state. Surface area versus cluster volume for each (c) oil and (d) CO_2 cluster and production step. Oil (e) and CO_2 (f) droplet capillary pressures. Measured at 323 K and 10-MPa pore pressure.

−100 to 200 kPa to −350 to 350 kPa but then stayed constant after waterflooding; this is clearly related to a broadening in curvature values of the oil drops. The p_c range for the CO_2 clusters did not significantly change and remained at ~−40 to 40 kPa. Note that the interfacial curvatures were similar for CO_2 and oil (ranging

Table 3
Statistical Parameters Associated With the Initial and Residual Oil and CO_2 Clusters for Each Production Step (Oil-Wet Bentheimer Sandstone, 318 K, 10-MPa Pore Pressure)

Production step		τ	p
S_{wc}	oil	1.09	0.79
	CO_2	—	—
S_{gi}	oil	1.30	0.79
	CO_2	1.10	0.85
S_{gr}	oil	1.35	0.85
	CO_2	1.20	0.85

from −15 to 15 μm^{-1}); thus, the large difference in the nominal values of the CO_2 and oil capillary pressures were caused by the significantly lower CO_2-oil interfacial tension.

3.4. Limitations

This study was conducted at typical μCT scale; that is, the observed volume was only several cubic millimeters (cf. e.g., Blunt et al., 2013 or Iglauer & Lebedev, 2018). At field scale, additional factors including geological reservoir features, or gravity effects play a significant role, and also need to be considered (e.g., Moortgat et al., 2011). Furthermore, the core was initially completely filled with oil (note that due to the strong hydrophobicity of the core it was not possible to 100% saturate it with water), which is only approximately representative of an oil reservoir core which also contains some water initially. However, the error in saturations is small. The subsequent coreflood sequence mimicked a scenario where CO_2 is directly injected into an oil reservoir, and the large number of PV used during the different flooding steps represents more the situation closer to the wellbore, while a smaller number of PV are expected to sweep deeper through the reservoir. This is, however, a limitation of the small sample used (as required by the μCT technology; Iglauer & Lebedev, 2018), and the associated very small fluid volumes (1 × PV = 40 μl). Note that no comparative study was conducted on an analogue water-wet sample (where different flow patterns are expected, e.g., Iglauer et al., 2013, Blunt, 2017), and only one full coreflood sequence was imaged with μCT.

4. Conclusions and Implications

CO_2 geosequestration in oil reservoirs is an attractive solution to dispose anthropogenic CO_2 while simultaneously enhancing oil recovery (Cantucci et al., 2009). However, the effectiveness of the three-phase (micrometer) pore-scale displacement mechanism, when CO_2 is injected into a formation, and additional oil is mobilized, is only poorly understood. We thus imaged such a displacement sequence at high resolution in situ in 3-D via X-ray μCT at reservoir conditions in an outcrop sandstone core. Significant amounts of residual CO_2 saturations were achieved in an oil-wet rock (13.5%), while oil production was enhanced substantially (~50% total oil recovery was achieved). Furthermore, the residual oil and CO_2 cluster size distributions, and the cluster surface area-volume relationships followed power law distributions, similar to the situation in two-phase flow despite three-phase flow being dramatically more complex (e.g., Øren et al., 1992). We conclude that, at the pore-scale, CO_2-EOR is an efficient method to residually trap CO_2 and recover significant incremental oil.

Acknowledgments
The measurements were performed using the μCT system courtesy of the National Geosequestration Laboratory (NGL) of Australia. The NGL is a collaboration between Curtin University, CSIRO, and the University of Western Australia established to conduct and deploy critical research and development to enable commercial-scale carbon storage options. Funding for this facility was provided by the Australian Federal Government. We would also like to thank the Pawsey supercomputer centre for access to Pawsey workstations and Avizo software. Adriana Paluszny thanks the Royal Society for funding through Fellowship UF160443. The μCT data are deposited in repository (https://www.digitalrocksportal.org/).

References

Al-Anssari, S., Barifcani, A., Wang, S., Lebedev, M., & Iglauer, S. (2016). Wettability alteration of oil-wet carbonate by silica nanofluid. *Journal of Colloid and Interface Science*, *461*, 435–442. https://doi.org/10.1016/j.jcis.2015.09.051

Al-Khdheeawi, E., Vaille, S., Sarmadivaleh, M., Barifcani, A., & Iglauer, S. (2017). Impact of reservoir wettability and heterogeneity on CO_2-plume migration and trapping capacity. *International Journal of Greenhouse Gas Control*, *58*, 142–158. https://doi.org/10.1016/j.ijggc.2017.01.012

Al-Menhali, A. S., & Krevor, S. C. (2016). Capillary trapping of CO_2 in oil reservoirs: observations in a mixed-wet carbonate rock. *Environmental Science & Technology*, *50*(5), 2727–2734. https://doi.org/10.1021/acs.est.5b05925

Al-Menhali, A. S., Menke, H. P., Blunt, M. J., & Krevor, S. C. (2016). Pore scale observations of trapped CO_2 in mixed-wet carbonate rock: Applications to storage in oil fields. *Environmental Science & Technology*, *50*(18), 10,282–10,290. https://doi.org/10.1021/acs.est.6b03111

Al-Yaseri, A., Lebedev, M., Barifcani, A., & Iglauer, S. (2016a). Receding and advancing CO_2-brine-quartz contact angles as a function of pressure, temperature, surface roughness and salinity. *Journal of Chemical Thermodynamics*, *93*, 416–423. https://doi.org/10.1016/j.jct.2015.07.031

Al-Yaseri, A. Z., Lebedev, M., Barifcani, A., & Iglauer, S. (2016b). Dependence of quartz wettability on fluid density. *Geophysical Research Letters*, *43*, 3771–3776. https://doi.org/10.1002/2016GL068278

Andrew, M., Bijeljic, B., & Blunt, M. J. (2013). Pore-scale imaging of geological carbon dioxide storage under in situ conditions. *Geophysical Research Letters*, *40*, 3915–3918. https://doi.org/10.1002/grl.50771

Andrew, M., Bijeljic, B., & Blunt, M. J. (2014). Pore-scale imaging of trapped supercritical carbon dioxide in sandstones and carbonates. *International Journal of Greenhouse Gas Control*, *22*, 1–14. https://doi.org/10.1016/j.ijggc.2013.12.018

Arif, M., Lebedev, M., Barifcani, A., & Iglauer, S. (2017). Influence of shale-total organic content on CO_2 geo-storage potential. *Geophysical Research Letters*, *44*, 8769–8775. https://doi.org/10.1002/2019GL073532

Armstrong, R. T., Porter, M. L., & Wildenschild, D. (2012). Linking porescale interfacial curvature to column-scale capillary pressure. *Advances in Water Resources*, *46*, 55–62. https://doi.org/10.1016/j.advwatres.2012.05.009

Bear, J. (1988). *Dynamics of fluids in porous media*. Courier Dover Publications.

Blunt, M. J., Bijeljic, B., Dong, H., Gharbi, O., Iglauer, S., Mostaghimi, P., et al. (2013). Pore-scale imaging and modelling. *Advances in Water Resources*, *51*, 197–216.
Blunt, M. J. (2017). *Multiphase flow in permeable media: A pore-scale perspective*. Cambridge: Cambridge University Press.
Buades, C. B., & Morel, J. M. (2005). A non-local algorithm for image denoising. Proc. IEEECVPR 2:60-65.
Cantucci, B., Montegrossi, G., Vaselli, O., Tassi, F., Quattrocchi, F., & Perkins, E. H. (2009). Geochemical modelling of CO_2 storage in deep reservoirs: The Weyburn Project (Canada) case study. *Chemical Geology*, *265*, 181–197.
Chaudhary, K., Bayani Cardenas, M., Wolfe, W. W., Maisano, J. A., Ketcham, R. A., & Bennett, P. C. (2013). Pore-scale trapping of supercritical CO_2 and the role of grain wettability and shape. *Geophysical Research Letters*, *40*, 1–5. https://doi.org/10.1002/grl.50658
Cuiec, L. E. (1991). Evaluation of reservoir wettability and its effect on oil recovery. In N. R. Morrow (Ed.), *Interfacial Phenomena in Petroleum Recovery* (Chap. 9, pp. 319–375). New York: Marcel Dekker.
El-Magrhaby, R., Pentland, C. H., Iglauer, S., & Blunt, M. J. (2012). A fast method to equilibrate carbon dioxide with brine at high pressure and elevated temperature including solubility measurements. *Journal of Supercritical Fluids*, *62*, 61–78.
Emami-Meybodi, H., Hassanzadeh, H., Green, C. P., & Ennis-King, J. (2015). Convective dissolution of CO_2 in saline aquifers: Progress in modeling and experiments. *International Journal of Greenhouse Gas Control*, *40*, 238–266. https://doi.org/10.1016/j.ijggc.2015.04.003
Emberley, S., Hutcheon, I., Shevalier, M., Durocher, K., Mayer, B., Gunter, W. D., & Perkins, E. H. (2005). Monitoring of fluid-rock interaction and CO2 storage through produced fluid sampling at the Weyburn CO2-injection enhanced oil recovery site, Saskatchewan. *Applied Geochemistry*, *20*(6), 1131–1157. https://doi.org/10.1016/j.apgeochem.2005.02.007
Geistlinger, H., & Mohammadian, S. (2015). Capillary trapping mechanism in strongly water-wet systems: Comparison between experiment and percolation theory. *Advances in Water Resources*, *79*, 35–50. https://doi.org/10.1016/j.advwatres.2015.02.010
Geistlinger, H., Mohammadian, S., Schlueter, S., & Vogel, H. J. (2014). Quantification of capillary trapping of gas clusters using x-ray microtomography. *Water Resources Research*, *50*, 4514–4529. https://doi.org/10.1002/2013WR014657
Georgiadis, A., Berg, S., Makurat, A., Maitland, G., & Ott, H. (2013). Pore-scale micro-computed tomography imaging: Non-wetting-phase cluster-size distribution during drainage and imbibition. *Physical Review E*, *88*(3). https://doi.org/10.1103/PhysRevE.88.033002
Green, D. W., & Willhite, G. P. (1998). Enhanced oil recovery, SPE Publications, Richardson.
Herring, A. L., Harper, E. J., Andersson, L., Sheppard, A., Bay, B. K., & Wildenschild, D. (2013). Effect of fluid topology on residual nonwetting phase trapping: Implications for geologic CO_2 sequestration. *Advances in Water Resources*, *62*, 47–58.
Iglauer, S. (2017). CO_2-water-rock wettability: Variability, influencing factors and implications for CO_2 geo-storage. *Accounts of Chemical Research*, *50*(5), 1134–1142. https://doi.org/10.1021/acs.accounts.6b00602
Iglauer, S., Al-Yaseri, A. Z., Rezaee, R., & Lebedev, M. (2015). CO_2-wettability of caprocks: Implications for structural storage capacity and containment security. *Geophysical Research Letters*, *42*, 9279–9284. https://doi.org/10.1002/2015GL065787
Iglauer, S., Favretto, S., Spinelli, G., Schena, G., & Blunt, M. J. (2010). X-ray tomography measurements of power-law cluster size distributions for the nonwetting phase in sandstones. *Physical Review E*, *82*(5), 056315. https://doi.org/10.1103/PhysRevE.82.056315
Iglauer, S., & Lebedev, M. (2018). High pressure-elevated temperature X-ray micro-computed tomography for subsurface applications. *Advances in Colloid and Interface Science*, *256*, 393–410. https://doi.org/10.1016/j.cis.2017.12.009
Iglauer, S., Paluszny, A., & Blunt, M. (2013). Simultaneous oil recovery and residual gas storage: a pore-level analysis using in-situ X-ray micro-tomography. *Fuel*, *1*, 1–11.
Iglauer, S., Paluszny, A., Pentland, C. H., & Blunt, M. J. (2011). Residual CO_2 imaged with X-ray micro-tomography. *Geophysical Research Letters*, *38*, L21403. https://doi.org/10.1029/2011GL049680
Iglauer, S., Pentland, C. H., & Busch, A. (2015). CO_2-wettability of seal and reservoir rocks and the implications for carbon geo-sequestration. *Water Resources Research*, *51*, 729–774. https://doi.org/10.1002/wrcr.21095
Iglauer, S., Sarmadivaleh, M., Al-Hinai, A., Ferno, M., & Lebedev, M. (2016). Influence of wettability on residual gas trapping and enhanced oil recovery in three-phase flow: a pore-scale analysis using micro-computed tomography. *SPE Journal*, *21*(06), 1916–1929. https://doi.org/10.2118/179727-PA
Iglauer, S., & Wülling, W. (2016). The scaling exponent of residual non-wetting phase cluster size distributions in porous media. *Geophysical Research Letters*, *43*, 11,253–11,260. https://doi.org/10.1002/2016GL071298
Intergovernmental Panel on Climate Change (2005). IPCC special report on carbon dioxide capture and storage, prepared by Working Group III of the Intergovernmental Panel on Climate Change, Cambridge University Press.
Jiang, L., Yu, M., Wu, B., Suekane, T., Li, W., & Song, Y. (2016). Characterization of dissolution process during brine injection in Berea sandstones: An experiment study. *RSC Advances*, *6*(115), 114,320–114,328. https://doi.org/10.1039/C6RA19024C
Karpyn, Z. T., Piri, M., & Singh, G. (2010). Experimental investigation of trapped oil clusters in a water-wet bead pack using x-ray microtomograph. *Water Resources Research*, *46*, W04510. https://doi.org/10.1029/2008WR007539
Keller, A. A., & Chen, M. (2003). Effect of spreading coefficient on three-phase relative permeability of nonaqeous phase liquids. *Water Resources Research*, *39*(10), 1288. https://doi.org/10.1029/2003WR002071
Khishvand, M., Alizadeh, A. H., & Piri, M. (2016). In-situ characterisation of wettability and pore-scale displacements during two- and three-phase flow in natural porous media. *Advances in Water Resources*, *97*, 279–298. https://doi.org/10.1016/j.advwatres.2016.10.009
Krevor, S., Blunt, M. J., Benson, S. M., Pentland, C. H., Reynolds, C., Al-Menhali, A., & Niu, B. (2015). Capillary trapping for geologic carbon dioxide storage—From pore scale physics to field scale implications. *International Journal of Greenhouse Gas Control*, *40*, 221–237. https://doi.org/10.1016/j.ijggc.2015.04.006
Lake, L.W. (2010). Enhanced oil recovery, Richardson: SPE Publications.
Li, X., Boek, E., Maitland, G. C., & Trusler, J. P. M. (2012). Interfacial tension of (brines + CO2): (0.864 NaCl + 0.136 KCl) at temperatures between (298 and 448) K, pressures between (2 and 50) MPa, and total molalities of (1 to 5) mol kg−1. *Journal of Chemical & Engineering Data*, *57*(4), 1078–1088. https://doi.org/10.1021/je201062r
Lorenz, C. D., & Ziff, R. M. (1998). Precise determination of the bond percolation thresholds and finite-size scaling corrections for the sc, fcc, and bcc lattices. *Physical Review E*, *57*(1), 230.
Moortgat, J., Sun, S., & Firoozabadi, A. (2011). Compositional modeling of three-phase flow with gravity using higher-order finite element methods. *Water Resources Research*, *47*, W05511. https://doi.org/10.1029/2010WR009801
Naylor, M., Wilkinson, M., & Haszeldine, R. S. (2011). Calculation of CO_2 column height in depleted gas fields from known pre-production gas column heights. *Marine and Petroleum Geology*, *28*(5), 1083–1093. https://doi.org/10.1016/j.marpetgeo.2010.10.005
Nwidee, L. N., Al-Anssari, S., Barifcani, A., Sarmadivaleh, M., Lebedev, M., & Iglauer, S. (2016). Nanoparticles influence on wetting behaviour of fractured limestone formation. *Journal of Petroleum Science and Engineering*, *149*, 782–788.
Øren, P. E., Billiote, J., & Pinczewski, W. V. (1992). Mobilization of waterflood residual oil by gas injection for water-wet conditions. *SPE Formation Evaluation*, *7*(01), 70–78. https://doi.org/10.2118/20185-PA

Øren, P. E., & Pinczewski, W. V. (1994). Effect of wettability and spreading on recovery of waterflooding residual oil by immiscible gas-flooding. *SPE Formation Evaluation*, *9*(02), 149–156. https://doi.org/10.2118/24881-PA

Øren, P.-E., & Pinczewski, W. V. (1995). Fluid distribution and pore-scale displacement mechanisms in drainage dominated three-phase flow. *Transport in Porous Media*, *20*(1-2), 105–133. https://doi.org/10.1007/BF00616927

Pentland, C. H., Okahabi, K., Suekane, T., & Iglauer, S. (2012). Influence of pore geometry on residual carbon dioxide trapping, 2012 SPE Asia Pacific Oil & Gas Conference and Exhibition, Perth, Australia, 22-24nd October 2012.

Piri, M., & Blunt, M. J. (2004). Three-phase threshold capillary pressures in noncircular capillary tubes with different wettabilities including contact angle hysteresis. *Physical Review E*, *70*(6), 061603. https://doi.org/10.1103/PhysRevE.70.061603

Rahman, T., Lebedev, M., Barifcani, A., & Iglauer, S. (2016). Residual trapping of supercritical CO_2 in oil-wet sandstone. *Journal of Colloid and Interface Science*, *469*, 63–68. https://doi.org/10.1016/j.jcis.2016.02.020

Saenger, E. H., Lebedev, M., Uribe, D., Osorno, M., Vialle, S., Duda, M., et al. (2016). Analysis of high-resolution X-ray computed tomography images of Bentheimer sandstone under elevated confining pressures. *Geophyscial Prospecting*, *64*(4), 848–859. https://doi.org/10.1111/1365-2478.12400

Sahimi, M. (2011). *Flow and transport in porous media and fractured rock*. Weinheim: Wiley-VCH. https://doi.org/10.1002/9783527636693

Scanziani, A., Singh, K., Bultreys, T., Bijeljic, B., & Blunt, M. J. (2018). In situ characterization of immiscible three-phase flow at the pore scale for a water-wet carbonate rock. *Advances in Water Resources*, *121*, 446–455. https://doi.org/10.1016/j.advwatres.2018.09.010

Schlüter, S., Sheppard, A., Brown, K., & Wildenschild, D. (2014). Image processing of multiphase images obtained via microtomography: A review. *Water Resources Research*, *50*, 3615–3639. https://doi.org/10.1002/2014WR015256

Soll, W. E., Celia, M. A., & Wilson, J. L. (1993). Micromodel studies of three-fluid porous media systems: pore-scale processes relating to capillary pressure-saturation relationships. *Water Resources Research*, *29*(9), 2963–2974. https://doi.org/10.1029/93WR00524

Span, R., & Wagner, W. (1996). A new equation of state for carbon dioxide covering the fluid region from the triple-point temperature to 1100 K at pressures up to 800 MPa. *Journal of Physical and Chemical Reference Data*, *25*(6), 1509–1596. https://doi.org/10.1063/1.555991

Stalker, L., Varma, S., Van Gent, D., Haworth, J., & Sharma, S. (2013). South West Hub: a carbon capture and storage project. *Australian Journal of Earth Sciences*, *60*(1), 45–58. https://doi.org/10.1080/08120099.2013.756830

Stauffer, D. (1979). Scaling theory of percolation clusters. *Physics Reports*, *54*(1), 1–74. https://doi.org/10.1016/0370-1573(79)90060-7

Watts, N. L. (1987). Theoretical aspects of caprock and fault seals for single- and two-phase hydrocarbon columns. *Marine and Petroleum Geology*, *4*(4), 274–307. https://doi.org/10.1016/0264-8172(87)90008-0

Yang, D., Gu, Y., & Tontiwachwuthikul, P. (2008a). Wettability determination of the reservoir brine−reservoir rock system with dissolution of CO_2 at high pressures and elevated temperatures. *Energy & Fuels*, *22*(1), 504–509.

Yang, D., Gu, Y., & Tontiwachwuthikul, P. (2008b). Wettability determination of the crude oil−reservoir brine−reservoir rock system with dissolution of CO_2 at high pressures and elevated temperatures. *Energy & Fuels*, *22*(4), 2362–2371.

Yang, D., Tontiwachwuthikul, P., & Gu, Y. (2005). Interfacial tensions of the crude oil + reservoir brine + CO_2 systems at pressures up to 31 MPa and temperatures of 27 °C and 58 °C. *Journal of Chemical & Engineering Data*, *50*(4), 1242–1249. https://doi.org/10.1021/je0500227